POAC'23
Glasgow, United Kingdom

Proceedings of the 27th International Conference on
Port and Ocean Engineering under Arctic Conditions
12-16 June 2023, Glasgow, United Kingdom

Analysis on the Influence of Measuring Point Failure in Ice Load Identification of Ship Structures

Jianwei Wang[1], Xiaodong Chen[1], Shunying Ji[1]
[1] State Key Laboratory of Structural Analysis, Optimization and CAE Software for Industrial Equipment, Dalian University of Technology, Dalian, China

ABSTRACT

The field measurement of ship structures is an important way to study ice loads. The aim of this study is to investigate the influence of measuring point failure in the ice load identification of ship structures and to propose effective method to considerably weaken this influence. According to both measured and simulated strain data of the icebreaker *Xue Long* 2, the spatial distribution characteristics of the identification error in the monitoring area are determined. According to the analysis of the strains at measuring points under typical load scenarios, the spatial distribution characteristics of the strains along frames are determined. On this basis, a least squares fitting method for estimating the strains at failed points is proposed. A practical solution to identify the ice load using the influence coefficient matrix method under the influence of measuring point failure is finally presented and discussed.

KEY WORDS: Ship structure; Ice load identification; Measuring point failure; Least squares fitting; Influence coefficient matrix.

INTRODUCTION

The field measurement of the ice load on ship structures has generated considerable recent research interest in ice engineering. Since the 1960s, a large number of field measurements have been carried out in the countries around the Arctic (Kotilainen et al., 2017; Li et al., 2018; Ralph et al., 2008; Kwon, Lee et al., 2015). In China, several field measurements of the ice-induced vibration and ice load on the icebreaker *Xue Long* were carried out during the research expeditions in the Antarctic and Arctic, and an ice load monitoring and alarm system (ILMS) was designed specifically for the icebreaker *Xue Long* 2. This system can make real-time feedback and assist decision-making on ice impact events in order to improve navigation safety in ice regions.

Ship-ice interaction is a complex dynamic coupling process (Huang et al., 2018; Lee et al., 2016). It is difficult to measure the ice load directly at present. By contrast, the strain caused by the ice load can be conveniently measured by strain sensors. Therefore, indirect methods are usually adopted, that is, ice loads are identified from the strains at measuring points. The

influence coefficient matrix (ICM) method is the most classic and widely adopted one (Lee et al., 2014; Suominen et al., 2017). The installation positions of strain sensors are generally concentrated on the frames, stringers, beams, plates, and other components at the side of bows or shoulders (Kotilainen et al., 2017; Ritch et al., 2008; Kwon, Choi et al., 2015).

In addition to errors, faults also exist in the data obtained from the field measurements of engineering structures in some cases. Fault data is largely caused by measuring point failure, thereby reducing the reliability of conclusions. In the field measurement of the ice load on ship structures, to be specific, the effectiveness of strain sensors directly determines the accuracy of identification results. However, few studies in the literature focused on the measuring point failure in the ice load identification of ship structures.

In the present study, this influence is studied based on the strain data of the icebreaker *Xue Long* 2. According to the spatial distribution characteristics of the strains at measuring points along frames, a least squares fitting method for the estimation of the strains at failed points is proposed. Consequently, a practical solution to identify the ice load under the influence of measuring point failure is presented and discussed.

INFLUENCE OF MEASURING POINT FAILURE IN ICE LOAD IDENTIFICATION

Description of the Ship and Instrumentation

Xue Long 2, China's first self-built icebreaker, is the world's first polar research vessel that adopts both stem and stern icebreaking technology. With the ice class of PC3, it is capable of continuously breaking ice at a speed of 2~3 kn in the environment of 1.5 m-thick ice with 0.2 m-thick snow. The ice load monitoring area of *Xue Long* 2 is set in Ballast Tank No. 10 on the starboard side of the stem shoulder. 88 measuring points are distributed on the webs of the 11 frames between Fr. 117 and 123, forming an array of fiber optic sensors with 8 rows and 11 columns. These sensors are used to measure the normal strain perpendicular to the hull plate, as shown in Figure 1.

Influence Coefficient Matrix Method for Ice Load Identification

The ICM method is based on the linear elasticity hypothesis and holds that there is a proportional relationship between ice-induced strains $\boldsymbol{\varepsilon}$ and ice loads $\boldsymbol{F}$ as follows:

$$\boldsymbol{\varepsilon} = \boldsymbol{\delta F} \Leftrightarrow \boldsymbol{F} = \boldsymbol{C\varepsilon} \tag{1}$$

where $\boldsymbol{C}$ is the stiffness matrix (i.e. the ICM), and $\boldsymbol{\delta}$ is the flexibility matrix. All elements in $\boldsymbol{\delta}$ can be determined by individually applying a unit load to each subarea in the monitoring area, as depicted in Figure 1. Finally, $\boldsymbol{F}$ can be identified by multiplying $\boldsymbol{C}$ by $\boldsymbol{\varepsilon}$.

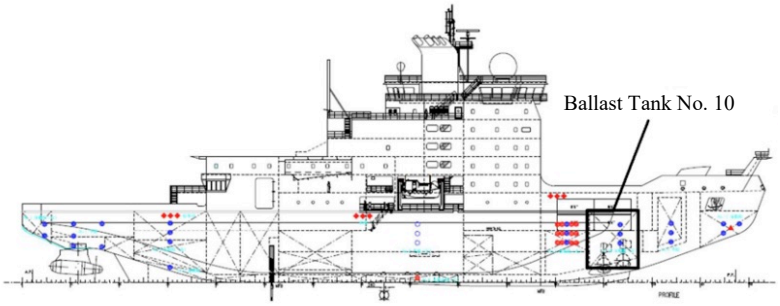

(a) Location of the ice load monitoring area

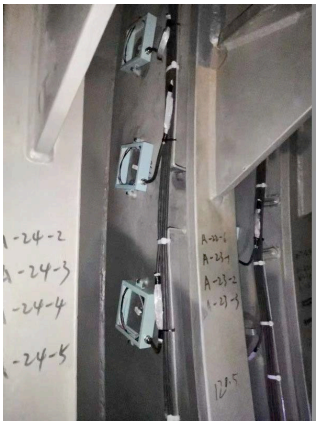

(b) Installation of fiber optic sensors

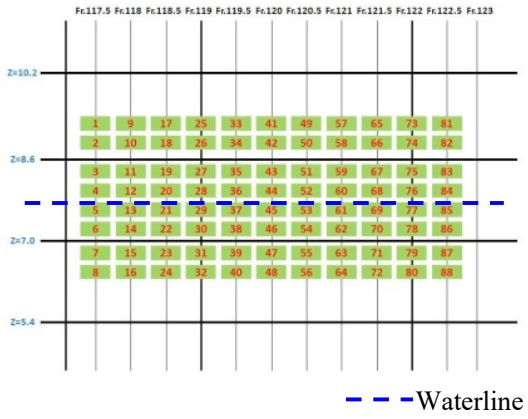

(c) Distribution of measuring points

Figure 1. Layout of the monitoring area and measuring points

Influence of Measuring Point Failure on Identification Results

According to the ICM method, the ice load in each subarea is identified from the measured ice-induced strain at each measuring point. An investigation of the strain data at the 88 measuring points of *Xue Long* 2 found that 17 points were failed during the 36th Chinese National Antarctic Research Expedition, as shown in Figure 2. Fortunately, they were timely restored before the 11th Arctic Research Expedition.

1	9	17	25	33	41	49	57	65	73	81
2	10	18	26	34	42	50	58	66	74	82
3	11	19	27	35	43	51	59	67	75	83
4	12	20	28	36	44	52	60	68	76	84
5	13	21	29	37	45	53	61	69	77	85
6	14	22	30	38	46	54	62	70	78	86
7	15	23	31	39	47	55	63	71	79	87
8	16	24	32	40	48	56	64	72	80	88

Original subarea Failed point

Figure 2. Distribution of the failed points in the monitoring area

In order to analyze the influence of these failed points on the identification result in each subarea, and to facilitate the study of the spatial distribution characteristics of the identification error in the monitoring area, a pressure of 2.5 MPa is applied to the entire monitoring area on the hull plate of the finite element model of *Xue Long* 2, see Figure 3. The strains at the failed points are replaced with zero. The identification error e_i in the subarea where Point i is located is written as follows:

$$e_i = \frac{\left|p_i' - p_i^{\text{real}}\right|}{p_i^{\text{real}}} \times 100\%, i = 1,2,\ldots,88 \tag{2}$$

where p_i' is the identified value of the ice load in the subarea where Point i is located, and

p_i^{real} is the ice load actual applied in the subarea. The spatial distribution of the identification error in the monitoring area is shown in Figure 4.

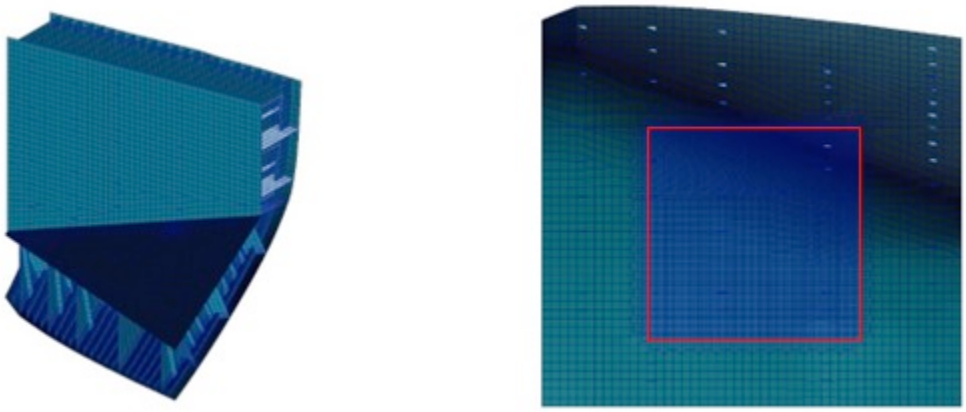

(a) Model overview (b) Monitoring area on the hull plate

Figure 3. The finite element model of the stem shoulder of *Xue Long* 2

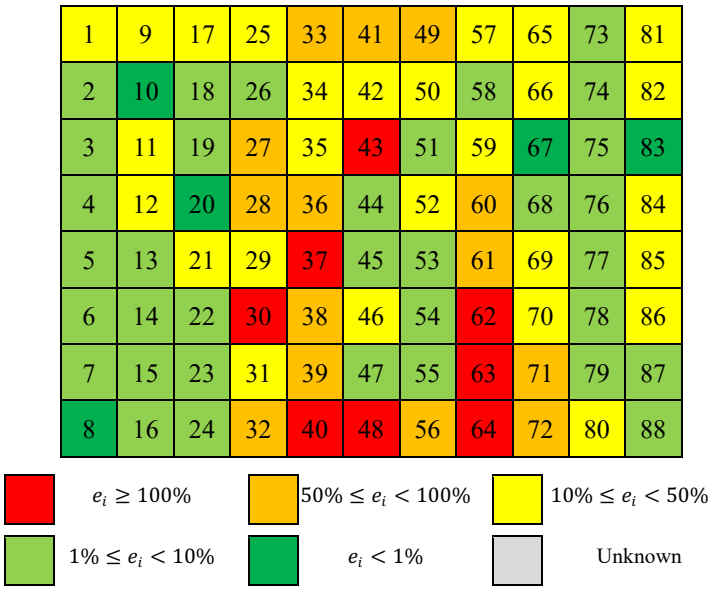

Figure 4. Spatial distribution of the identification error in the monitoring area

Figure 4 shows that the impact of measuring point failure on identification results is significant. In general, the closer the subarea is to the failed points, the greater the identification error. The subarea where the failed point is located exhibits the largest error, but there may be a subarea near the failed point, such as Point 44, where the error is small. For the subarea, such as Area 5, that is separated from the failed points by more than two subareas, this influence can be ignored.

ICE LOAD IDENTIFICATION METHOD BASED ON LEAST SQUARES FITTING

Least Squares Method for the Fitting of Strains at Measuring Points

For the given strain data $\{(X_i, \varepsilon_i), i = 0,1, \ldots, m\}$ (where X_i is the coordinate of the measuring point, and ε_i is the strain at the measuring point), try to find $\varepsilon^*(X)$ in $\varepsilon(X)$ in the form of Eq. (4) to minimize the sum of squared errors $\|\boldsymbol{r}\|_2^2$, that is:

$$\|\boldsymbol{r}\|_2^2 = \sum_{i=0}^{m} r_i^2 = \sum_{i=0}^{m}[\varepsilon^*(X_i) - \varepsilon_i]^2 = \min_{\varepsilon(X)\in\varphi} \sum_{i=0}^{m}[\varepsilon(X_i) - \varepsilon_i]^2 \quad (3)$$

$$\varepsilon(X) = a_0\varphi_0(X) + a_1\varphi_1(X) + \cdots + a_n\varphi_n(X) \quad (4)$$

where $\varphi_0(X), \varphi_1(X), \ldots, \varphi_n(X)(n < m)$ are the family of linear independent functions on the continuous function space $C[a, b]$, and $a_0, a_1, \ldots, a_n$ are undetermined coefficients.

Eq. (3) can be transformed into the problem of seeking the minimum point $\boldsymbol{a}^* = (a_0^*, a_1^*, \ldots, a_n^*)^{\mathrm{T}}$ of the multivariate function shown in Eq. (5):

$$I(a_0, a_1, \ldots, a_n) = \sum_{i=0}^{m}\left[\sum_{j=0}^{n} a_j\varphi_j(X_i) - \varepsilon_i\right]^2 \quad (5)$$

The necessary condition for determining the extreme value of multivariate function is listed as follows:

$$\frac{\partial I}{\partial a_k} = 2\sum_{i=0}^{m}\left[\sum_{j=0}^{n} a_j\varphi_j(X_i) - \varepsilon_i\right]\varphi_k(X_i) = 0 \quad (6)$$

If

$$\left(\varphi_j, \varphi_k\right) = \sum_{i=0}^{m} \varphi_j(X_i)\,\varphi_k(X_i) \quad (7)$$

$$(\varepsilon, \varphi_k) = \sum_{i=0}^{m} \varepsilon_i\,\varphi_k(X_i) \equiv d_k \quad (8)$$

Eq. (6) will be written as follows:

$$\sum_{j=0}^{n}\left(\varphi_j, \varphi_k\right)a_j = d_k, k = 0,1, \ldots, n \quad (9)$$

For the given strain data $\{(X_i, \varepsilon_i), i = 0,1, \ldots, m\}$, consider $\varphi = \mathrm{span}\{1, X, \ldots, X^n\}$. $\left(\varphi_j, \varphi_k\right)$ and (ε, φ_k) are derived from Eq. (7) and Eq. (8), and then substitute them into Eq. (9) to get $\boldsymbol{a}^*$. Finally, the least squares solution of $\varepsilon(X)$ can be expressed as follows:

$$\varepsilon^*(X) = a_0^* + a_1^*X + \cdots + a_n^*X^n \quad (10)$$

which is the analytic expression of the least squares fitting curve for the given strain data.

The goodness of fit (GOF) refers to the degree to which the fitting curve fits the data. The statistic that measures the GOF is the coefficient of determination, that is, R^2. The closer R^2 is to 1, the higher the GOF. If the mean and fitted values of the strain $\varepsilon_i(i = 0,1, \ldots, m)$ are represented as $\bar{\varepsilon}$ and $\hat{\varepsilon}_i$, R^2 will be written as follows:

$$R^2 = \frac{\sum_{i=0}^{m}(\hat{\varepsilon}_i - \bar{\varepsilon})^2}{\sum_{i=0}^{m}(\varepsilon_i - \bar{\varepsilon})^2} = 1 - \frac{\sum_{i=0}^{m}(\varepsilon_i - \hat{\varepsilon}_i)^2}{\sum_{i=0}^{m}(\varepsilon_i - \bar{\varepsilon})^2} \quad (11)$$

Spatial Distribution Characteristics of the Strains at Measuring Points

In order to study the spatial distribution characteristics of the strains at measuring points, uniform and nonuniform pressures are applied to the ice belt region of *Xue Long* 2 to simulate the real local ice load under different ice thicknesses, as shown in Figure 5. To avoid the influence of the stringers at $z = 8.6$ and 7.0, and the boundaries at Fr. 117 and 123, the strains at measuring points in the three strakes of the ice belt region, that is, the points in Rows 3~6

and Columns 2~10 are investigated, see Figure 1(c).

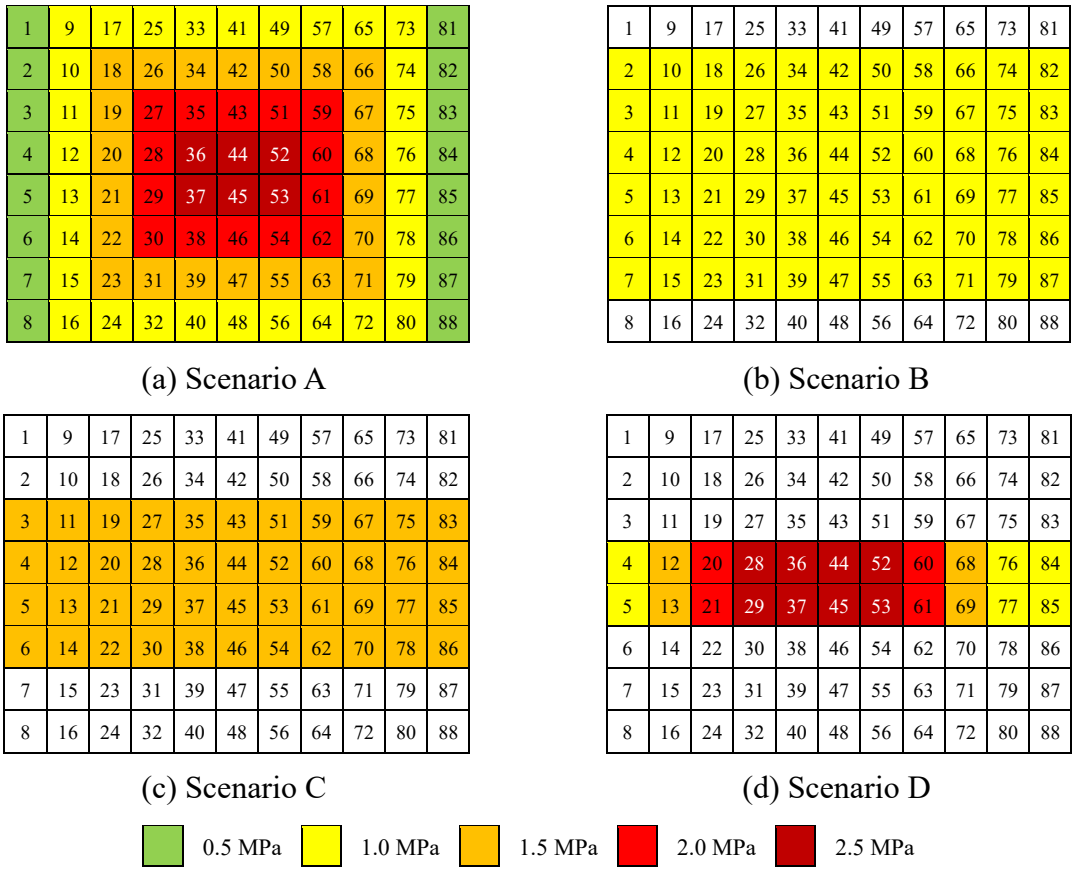

Figure 5. Typical load scenarios with uniform or nonuniform pressures

The quadratic polynomial is adopted as the fitting function of the strains at measuring points, that is, consider $\varphi = \mathrm{span}\{1, X, X^2\}$. The least squares fitting (LSF) is carried out according to Eqs. (7)~(10), and R^2 is calculated by Eq. (11) to investigate the GOF. The R^2 under typical load scenarios is listed in Table 1.

Table 1. R^2 of each group under typical load scenarios

Column No.	R^2			
	Scenario A	Scenario B	Scenario C	Scenario D
2	0.945	0.945	0.965	0.956
3	0.979	0.973	0.973	0.995
4	0.933	0.949	0.987	0.999
5	0.955	0.954	0.968	0.995
6	0.981	0.976	0.987	0.983
7	0.999	0.996	0.999	0.958
8	0.999	0.999	0.999	0.943
9	0.989	0.992	0.995	0.926
10	0.996	0.931	0.951	0.985

It is found that the R^2 of each group is close to 1, which shows that the quadratic function can reasonably describe the relationship between the strains and positions of measuring points. Moreover, load scenarios with different loading centers, ranges, and aspect ratios have little effect on the characteristics, so does the nonuniformity of localized ice loads.

Ice load identification under the influence of measuring point failure

According to the above analysis, the quadratic polynomial is adopted as the fitting function. According to Eqs. (7)~(10), the expression of the strain with respect to its position established by the LSF is expressed as follows:

$$\varepsilon^*(X) = a_0^* + a_0^* X + a_0^* X^2 \tag{12}$$

Substituting the coordinate of the failed point X_F into Eq. (12), the fitted value of the strain ε_F at this point can be obtained by Eq. (13):

$$\varepsilon_\mathrm{F} = a_0^* + a_0^* X_\mathrm{F} + a_0^* X_\mathrm{F}^2 \tag{13}$$

In order to effectively identify the ice load on *Xue Long* 2 under the influence of measuring point failure, the following solution is proposed: Estimate the strains at the failed points in the ice belt region by the LSF method. For other failed points that cannot be estimated due to the lack of points for fitting, redivide the monitoring area by combining the two subareas where the failed point and adjacent functional one are located. Then, select the strain at the functional point in the new subarea to identify the ice load. It should be noted that when subareas are removed or combined, the ICM should be reformed. The schematic diagram of the solution is shown in Figure 6.

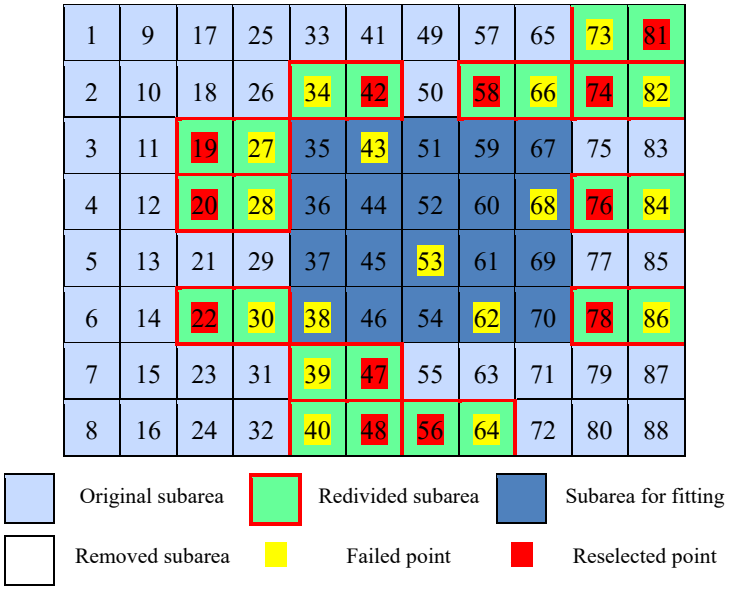

Figure 6. Schematic diagram of the solution to the ice load identification of *Xue Long* 2

DISCUSSION ON THE IDENTIFICATION EFFECT UNDER TYPICAL LOAD SCENARIOS

Under typical load scenarios, the comparison between the identified and true values of ice loads is shown in Figure 7. The spatial distribution of the identification error in the monitoring area

before and after adopting the solution is depicted in Figure 8.

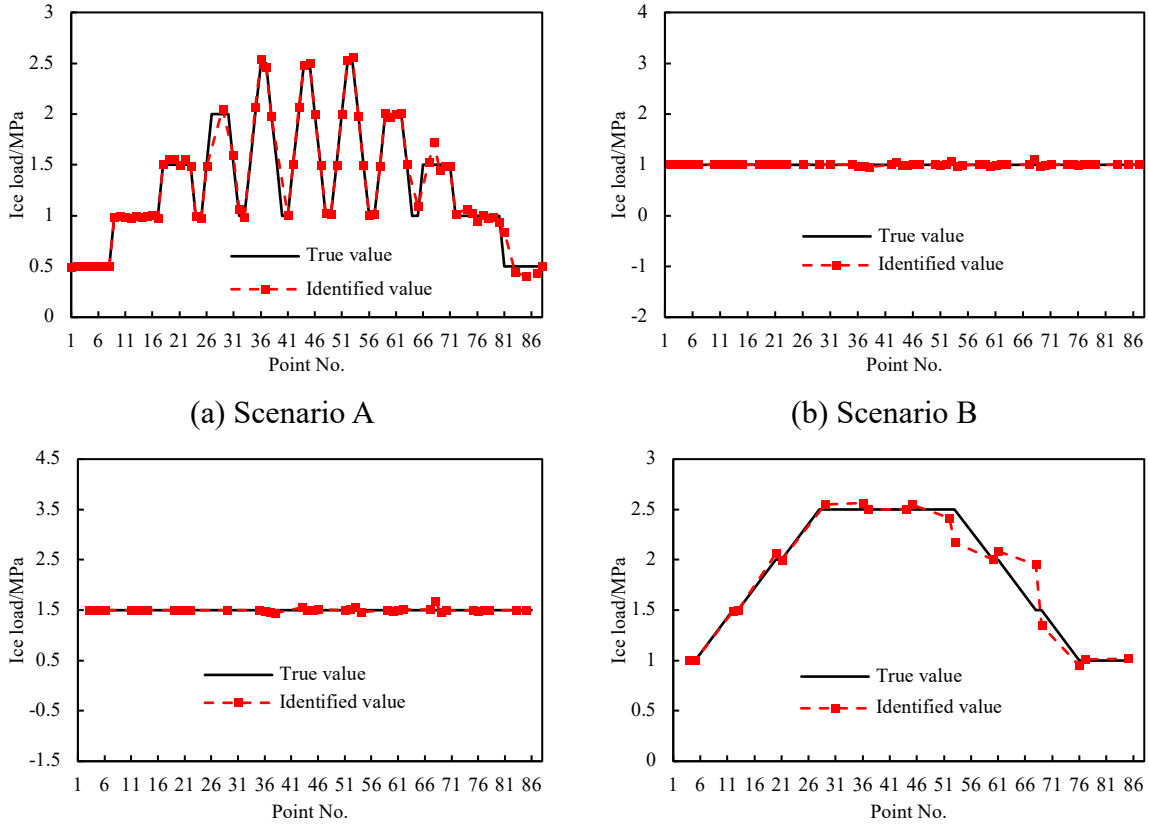

(a) Scenario A (b) Scenario B

(c) Scenario C (d) Scenario D

Figure 7. Comparison between the identified values and true values of ice loads

1	9	17	25	33	41	49	57	65	73	81
2	10	18	26	34	42	50	58	66	74	82
3	11	19	27	35	43	51	59	67	75	83
4	12	20	28	36	44	52	60	68	76	84
5	13	21	29	37	45	53	61	69	77	85
6	14	22	30	38	46	54	62	70	78	86
7	15	23	31	39	47	55	63	71	79	87
8	16	24	32	40	48	56	64	72	80	88

1	9	17	25	33	41	49	57	65	73	81
2	10	18	26	34	42	50	58	66	74	82
3	11	19	27	35	43	51	59	67	75	83
4	12	20	28	36	44	52	60	68	76	84
5	13	21	29	37	45	53	61	69	77	85
6	14	22	30	38	46	54	62	70	78	86
7	15	23	31	39	47	55	63	71	79	87
8	16	24	32	40	48	56	64	72	80	88

(a) Scenario A

1	9	17	25	33	41	49	57	65	73	81
2	10	18	26	34	42	50	58	66	74	82
3	11	19	27	35	43	51	59	67	75	83
4	12	20	28	36	44	52	60	68	76	84
5	13	21	29	37	45	53	61	69	77	85
6	14	22	30	38	46	54	62	70	78	86
7	15	23	31	39	47	55	63	71	79	87
8	16	24	32	40	48	56	64	72	80	88

1	9	17	25	33	41	49	57	65	73	81
2	10	18	26	34	42	50	58	66	74	82
3	11	19	27	35	43	51	59	67	75	83
4	12	20	28	36	44	52	60	68	76	84
5	13	21	29	37	45	53	61	69	77	85
6	14	22	30	38	46	54	62	70	78	86
7	15	23	31	39	47	55	63	71	79	87
8	16	24	32	40	48	56	64	72	80	88

(b) Scenario B

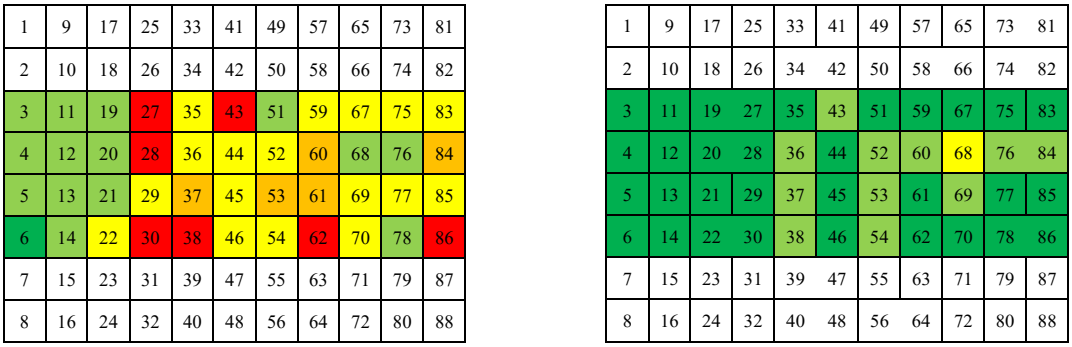

(c) Scenario C

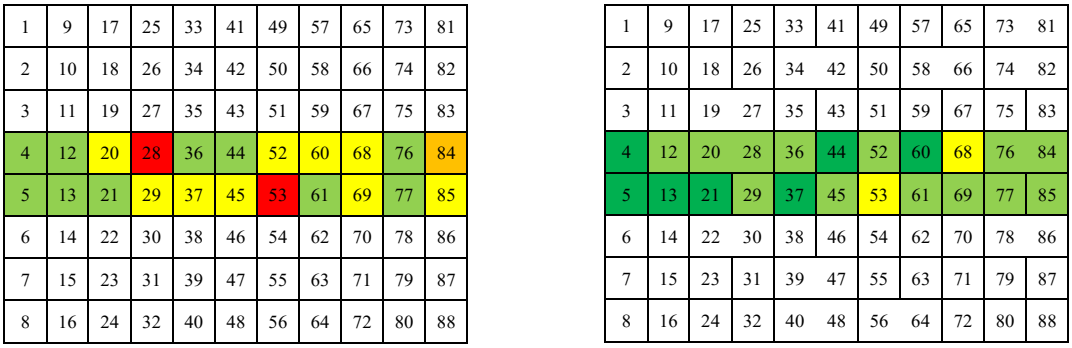

(d) Scenario D

Figure 8. Spatial distribution of the identification error in loading area before and after adopting the solution under typical scenarios

According to the above figures, the adoption of the solution greatly reduces the identification error and resulting in high fineness. Furthermore, the adoption of the LSF method for the estimation of the strains at failed points significantly weakens the influence of measuring point failure on identification results. The proportion of the error ranges of $e_i < 1\%$ and $1\% \leq e_i < 10\%$ in subareas is greatly increased and occupies the overwhelming majority. In contrast, there is almost no error ranges of $50\% \leq e_i < 100\%$ or $e_i \geq 100\%$.

CONCLUSIONS

Measuring point failure is a common situation in the field measurement of ship structures. This can make a significant impact on the ice load identification by the ICM method, but few studies in the literature have focused on this issue before. In this paper, the influence of measuring point failure is systematically investigated based on the icebreaker *Xue Long* 2, and an effective method is proposed to considerably weaken this influence.

The main conclusions are as follows:

(1) The influence of measuring point failure on the ice load identification of ship structures is considerable. The closer the subarea is to failed points, the greater the identification error. The subarea where the failed point is located exhibits the largest error. For the subareas that are separated from failed points by more than two subareas, this influence can be ignored.

(2) The LSF method can be used to estimate the strains at failed points. The quadratic function can reasonably describe the relationship between the strains and positions of measuring points. Load scenarios with different loading centers, ranges, and aspect ratios have little effect on the spatial distribution characteristics of the strains at measuring points, so does the nonuniformity

of localized ice loads.

(3) The LSF method for the estimation of the strains at failed points adopted in the solution can obviously decrease the identification error, thereby significantly weaken the influence of measuring point failure. In future research, the engineering reliability of the method proposed in this paper need to be further verified in the field measurements of more polar ships.

ACKNOWLEDGEMENTS

This work was supported by the National Natural Science Foundation of China [Grant Nos. 42176241, 52192693, U20A20327] and the High-Tech Ship Project of the Ministry of China [2021-342].

REFERENCES

Huang, Y., Huang, S., Sun, J., 2018. Experiments on navigating resistance of an icebreaker in snow covered level ice. *Cold Regions Science and Technology*, 152, pp.1-14.

Kotilainen, M., Vanhatalo, J., Suominen, M., Kujala, P., 2017. Predicting ice-induced load amplitudes on ship bow conditional on ice thickness and ship speed in the Baltic Sea. *Cold Regions Science and Technology*, 135, pp.116-126.

Kwon, Y.H., Choi, K., Lee, T.K., 2015. A study on statistical analysis of local ice loads measured during the arctic voyage of the IBRV ARAON. *Journal of Advanced Research in Ocean Engineering*, 1(3), pp.186-197.

Kwon, Y.H., Lee, T.K., Choi, K., 2015. A study on measurements of local ice pressure for ice breaking research vessel "Araon" at the Amundsen Sea. *International Journal of Naval Architecture and Ocean Engineering*, 7, pp.490-499.

Lee, J.H., Kwon, Y.H., Rim, C.W., Lee, T.K., 2016. Characteristics analysis of local ice load signals in ice-covered water. *International Journal of Naval Architecture and Ocean Engineering*, 8, pp.66-72.

Lee, T.K., Lee, J.H., Kim, H., Rim, C.W., 2014. Field measurement of local ice pressures on the Araon in the Beaufort Sea. *International Journal of Naval Architecture and Ocean Engineering*, 6(4), pp.788-799.

Li, F., Goerlandt, F., Kujala, P., Lehtiranta, J., Lensu, M., 2018. Evaluation of selected state-of-the-art methods for ship transit simulation in various ice conditions based on full-scale measurement. *Cold Regions Science and Technology*, 151, pp.94-108.

Ralph, F., McKenna, R., Gagnon, R., 2008. Iceberg characterization for the bergy bit impact study. *Cold Regions Science and Technology*, 52, pp.7-28.

Ritch, R., Frederking, R., Johnston, M., Browne, R., Ralph, F., 2008. Local ice pressures measured on a strain gauge panel during the CCGS Terry Fox bergy bit impact study. *Cold Regions Science and Technology*, 52(1), pp.29-49.

Suominen, M., Kujala, P., Romanoff, J., Remes, H., 2017. Influence of load length on short-term ice load statistics in full-scale. *Marine Structures*, 52, pp.153-172.